Contact behaviour and vibrational response of a high-speed train brake friction block

Z.Y. Xiang [a], J.L. Mo [a]*, H. Ouyang [b], F. Massi [c], B. Tang [a], Z.R. Zhou [a]

[a] Tribology Research Institute, School of Mechanical Engineering, Southwest Jiaotong University, Chengdu 610031, China

[b] School of Engineering, University of Liverpool, Liverpool L69 3GH, UK

[c] DIMA, Department of Mechanical and Aerospace Engineering, University of Rome "La Sapienza", Italy

* Corresponding author: jlmo@swjtu.cn (J.L. Mo).

ABSTRACT: Brake experiments were conducted on a typical kind of friction blocks of a high-speed train. The friction and wear, interfacial temperature, vibration, and noise generated at or by the brake interface were investigated, and the interrelationship between the vibration response and the contact behaviour of interface was analysed. The results showed the friction coefficient, vibration energy, and noise intensity were lower when the block surface experiences less wear; the friction coefficient and contact angle of the block were important factors affecting the vibration characteristics of the brake system. Moreover, the contact inclination angle increased with the increase in the friction coefficient, and mode coupling of the brake system occurred; as a result, the vibration intensity increased, and squeal occurred.

Keywords: Friction-induced vibration, contact behaviour, vibration response, experimental analysis, numerical analysis

1 INTRODUCTION

Due to the rapid development of high-speed railway systems and increased environmental requirements, friction-induced vibrations and noise (FIVN) from braking systems of high-speed trains has become a topic of increased interest for researchers and manufacturers of brake components, particularly brake pads or friction blocks [1-4]. Continuous and strong vibration exacerbates interface wear, causes crack initiation and reduces the service life of brake pads, which significantly affects the operational safety and reliability of the braking systems [5-8]. In addition, the emitted high-frequency squeal noise (>1000 Hz) can affect the comfort of passengers, and surrounding environment, resulting in dissatisfaction. Therefore, minimizing FIVN in railway brake systems is significant to the future development of high-speed trains.

Many studies have been conducted to investigate FIVN of the disc brake systems of high-speed trains [9-12], and several methods have been proposed to reduce FIVN [13-17]. It has been verified that tailoring the mechanical properties of key brake components is an effective method to reduce FIVN, such as modifying the structure of the brake pairs [18-21], optimizing the brake parameters [22], adjusting the contact stiffness of the brake system [23, 24], verifying the interface frictional excitation [25], and the use of damping [26-28]. These methods are effective for reducing the vibration intensity of brake systems under certain operating conditions, but may not have the same effect under different operating conditions. Therefore, it is insufficient to merely consider the vibration issues of brake systems as a dynamic behaviour, while ignoring the fact that a braking process is a

complex tribological problem due to oxidation reaction, thermal effects, and the physical and chemical changes that occur at the contact interface [29-33]. This has been recognized by researchers, and the effect of interfacial factors on the vibration response has been investigated in recent years.

To date, researchers have analysed the relationship between interfacial friction factors, including the friction force [34-37], contact stiffness [23, 24, 38-41], friction noise [25], contact inclination angle [42, 43], contact area [44-48], contact stress distribution [49-51], and the stability and vibration intensity of brake systems using experimental and numerical methods [52]. Yoon et al. [53] analysed the relationship between the surface topography of the pad and friction-induced vibration; the results indicated that the frequency response of the friction-induced vibration and its intensity were significantly influenced by the failure strength and stiffness of the contact areas. Bergman et al. [54] studied the influence of the contact area on the friction characteristics and the generation of squeal noise of friction systems. Similarly, the effect of the contact area on the velocity weakening of the friction coefficient was investigated by Kim et al [46], who also examined the noise-triggering mechanism of a brake system. Massi et al. [55] found that material exfoliation on worn surfaces was correlated with squeal noise occurrence, while friction noise generated by the interface phenomena were correlated with squeal triggering [25]. In these studies, the analysis of the interface characteristics showed that the contact areas of the friction pair had different sizes and shapes; since the contact area was the primary region of pressure and sliding, changes in the shape and size of the contact area affected brake vibration and noise.

These afore-mentioned findings indicate that the interface features of a friction system are important factors affecting the contact behaviour of the brake interface, and also affect the generation and evolution of FIVN. These researches mainly focus on the influence mechanisms of the interfacial factors and their association with the vibration response of brake systems. However, considering the complexity of the interfacial contact behaviour [31, 45, 53] and the randomness of the vibration response [56], it is important to investigate the relationship between them and their interaction mechanism. Especially for railway brake systems, they operate in more complex and varying operational environments, so that generated squeal events become more unpredictable and complex; consequently, the research findings gained from automobile brake systems should not be directly applicable to high-speed train brake systems.

In this work, the interrelationship between the contact behaviour and the vibration response of a high-speed train brake system was investigated experimentally and numerically. A series of brake tests were conducted at different disc rotation speeds using a brake dynamometer to reproduce different contact conditions and vibration characteristics. The observed surface topography and the contact pressure distribution on the friction block surface were correlated with the vibration response of the brake system. Complex eigenvalue analysis (CEA) as well as transient dynamic analysis (TDA) were performed by finite element method to explore the evolution of the correlation between the contact behaviour and the vibration response of the system. The results of this study highlighted the correlation between the tribological behaviour of the brake interface and the vibrational response of the brake system, and effective solutions should be taken to reduce the contact inclination angle of the friction block and spread the interface contact stress to avoid regions of concentrated contact stress. This study provided useful information to reduce FIVN of high-speed railway brake systems.

2 EXPERIMENTAL APPROACH

2.1 Details of the test setup

In this work, a self-designed small-scale brake dynamometer was used to study the relationship between the contact behaviour of the friction interface and the vibration response of the system at different disc rotation speeds. The dynamometer was used to simulate the disc-friction block contact behaviour of a real brake system of high-speed trains and reproduce the vibration response, which was able to explore the correlation between the contact behaviour and vibration response. The standard TJ/CL 310-2014 (a provisional specification for brake pads of Electric Multiple Units (EMU) in China) was adopted in the brake testing. The schematic diagram of the brake dynamometer is shown in Fig. 1.

The tribological response and the vibration and noise characteristics were obtained by pushing the friction block into contact with the rotating disc. The experimental dynamometer was driven by an AC motor (11 kW WIN-V63AC) with a maximum torque of 413 Nm. An accelerometer was installed on the block holder to measure the vibration accelerations generated at the friction interface, and a torque sensor was installed at the disc shaft to record the brake torque. A microphone was placed approximately 20 cm from the brake disc and was used to record the noise signals generated during the tests, which could ensure good quality in noise measurement and prevent wear debris from falling into the microphone during the brake testing. The time signals were acquired by a data acquisition system. The thermal characteristics of the disc and friction block surface were monitored by an infrared camera during the tests. A pressure film was used to measure the pressure at the contact interface after the braking tests were done. More information about the scaled brake dynamometer can be found in Ref. [19].

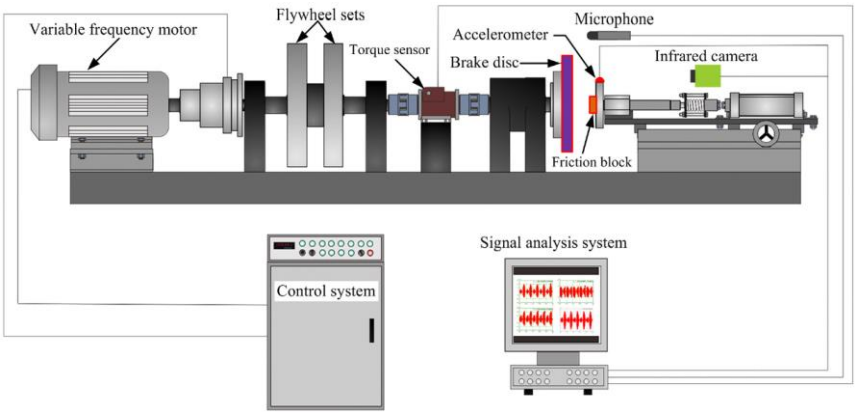

Fig. 1 Schematic diagram of the brake dynamometer [19]

2.2 Preparation of test materials

The disc and friction block samples used in this work were of the same materials as the real brake discs and pads of the China Railway High-speed (CRH) train braking system. It is noteworthy that the brake pads on high-speed trains possess many friction blocks with varied geometrical shapes [19], such as hexagonal, circular, elliptic, and triangular. The shape and the material of the scaled friction block samples were the same as those of the friction block in the train model CRH380A. The shape, size, and contact of the disc and friction block samples are illustrated in Fig. 2. The nominal contact area between the brake disc and the friction block sample was 731.7 mm^2. The material of the brake disc was forged steel (the chemical compositions as shown in Table 1) and the friction block was copper-based powder metallurgy material (the chemical compositions are shown in Table 2);

the mechanical and physical properties of the frictional materials are shown in Table 3.

In order to ensure the same initial surface status of the different friction block samples, a preliminary treatment was conducted before testing each friction block. First, all friction block surfaces were polished using the same process. Second, the polished friction blocks were placed in alcohol, treated ultrasonically for 3 minutes, and air-dried.

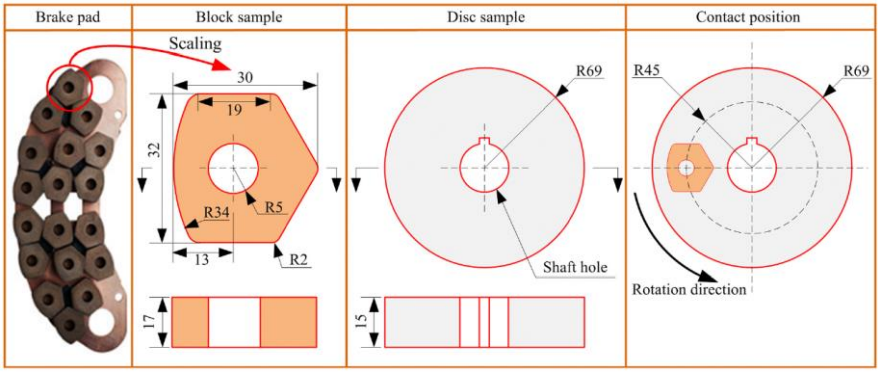

Fig. 2 Schematics of the brake disc and friction block samples

Table 1 Chemical compositions of the brake disc sample

Element	C	Si	Mn	Cr	Ni	Mo	Fe
Content (wt%)	0.31	0.25	0.75	1.1	1.8	0.5	Balance

Table 2 Chemical compositions of the friction block sample

Element	Cu	Fe	Graphite	MoS_2	FeCr	Sic	others
Content (wt%)	45-50	13-15	18-20	4-6	6-8	2-4	3-5

Table 3 Mechanical and physical properties of the frictional materials

Samples	Brake disc	Friction block
Density (kg/m^3)	7850	5200
Young's modulus (GPa)	210	6.5
Poisson ratio	0.3	0.29
Heat conductivity (W/(m•K))	32.2	40
Coefficient of linear expansion (1/°C)	1.16×10^{-5}	1.1×10^{-5}
Specific heat capacity (J/(kg•K))	480	534

Surface hardness (HB)	342	15-25

2.3 Test protocol

All brake disc and friction block samples underwent a running-in procedure prior to each group of tests to ensure good surface-to-surface contact. The contact area was defined as the region of the friction block surface, which was in contact with the brake disc surface and on which wear debris accumulation occurred and wear scratches were observed. During the running-in of each friction block, pauses were introduced at regular intervals to make sure that the friction block was not over-heated and its contact surface was visually inspected. When the rubbed area on the contact surface reaches 85%, as recommended in the standard TJ/CL 310-2014, the running-in was complete.

It is known that the vibration and squeal noise of railway brakes is more likely to occur at low speeds, especially from 30 km/h to final stop. That is why the brake squeal is usually heard as the train enters the station. Moreover, it is worth noting that the braking forces and speeds are changing all the time during the braking process of a high-speed train. Therefore, to ensure the equivalent linear velocity at the mean friction radius between the simulated and actual conditions, testing speed range of 200 rpm~400 rpm was selected to simulate the actual train speed range of about 6 km/h~12 km/h, in which friction-induced vibration and squeal noise of brake interface usually occurred. Based on the criterion of equal average contact pressure at the friction interface between simulated and actual conditions, testing load of 190 N was selected to simulate the actual train brake force of about 5.2 kN (according to the standard TJ/CL 310-2014).

The test time was 120 s to ensure steady-state behaviour of vibration acceleration and sound pressure signal, and progressive change of surface morphology of the friction block. All tests were performed at an ambient temperature of 20-27 °C and relative humidity of 62-70%. Each test was repeated at least five times to ensure the repeatability and reliability of the test results.

3 EXPERIMENTAL RESULTS AND DISCUSSION

3.1 Vibration and noise characteristics

The time-domain signals of the measured sound pressure and tangential acceleration and the fast Fourier transform (FFT) of these signals were obtained during 5 seconds of steady-state stage (53~58 s), to evaluate the vibration and noise characteristics of the brake system at three different brake disc rotation speeds; the results are shown in Fig. 3. The results show that the sound pressure and vibration signals exhibited consistency during the test, and the brake disc rotation speed significantly affected the sound pressure and vibration intensity, as shown in Fig. 3(a) and (b). FIVN signals were observed at all brake disc rotation speeds. Among them, there was an obvious intermittent vibration phenomenon under the brake disc rotation speed of 200 and 300rpm, which resulted in a similar phenomenon of sound pressure signal, while this phenomenon was not obvious at 400 rpm. Additionally, the RMS values of vibration acceleration and sound pressure signals in Fig. 3 (a) and (b) were calculated. The RMS values of the tangential vibration acceleration of the friction block at brake disc rotation speed of 200, 300 and 400 rpm were: 2246.4 m/s2, 1237.6 m/s2 and 534.4 m/s2, respectively; the RMS values of the sound pressure signal were: 11.7 Pa, 5.3 Pa and 2.1 Pa, respectively. These results show that, the higher the

brake disc rotation speed, the lower the sound pressure level was and the weaker the vibration was, at a given rotation.

Figure 3 (c) and (d) show the FFT analysis results of the sound pressure and vibration signals, respectively. It was found that the vibration signals contained a significant frequency of 8008 Hz, which was not present in the noise signals. It was found through measurement of motor vibration without brake application that this frequency was due to the motor vibration, which did not emit sound during brake tests. The spectra of the vibration and sound pressure with different rotation speeds were obviously different. The tangential vibration signals and the noise signals shared the same dominant frequency. Therefore, it can be deduced that these unstable vibrations originated from the mode coupling between the friction block and brake disc, emitting noise with identical frequencies (e. g. the peaks can be found in the frequency spectrum at 6641, 7129 and 13875 Hz under the brake disc rotation speed of 200 rpm, and 6763, 10238 and 13705 Hz for the case of 300 rpm). However, when the brake disc rotated at a speed of 400 rpm, the tangential vibration signal and the noise signal only had one common frequency (13624 Hz) which may also have resulted from the mode coupling between the friction block and brake disc.

Additionally, the frequencies of 13875, 13705, and 13624 Hz were the dominant frequencies of the sound pressure and vibration signals at brake disc rotation speeds of 200, 300, and 400 rpm, respectively. The dominant frequency and the amplitude decrease with an increase in the brake disc rotation speed.

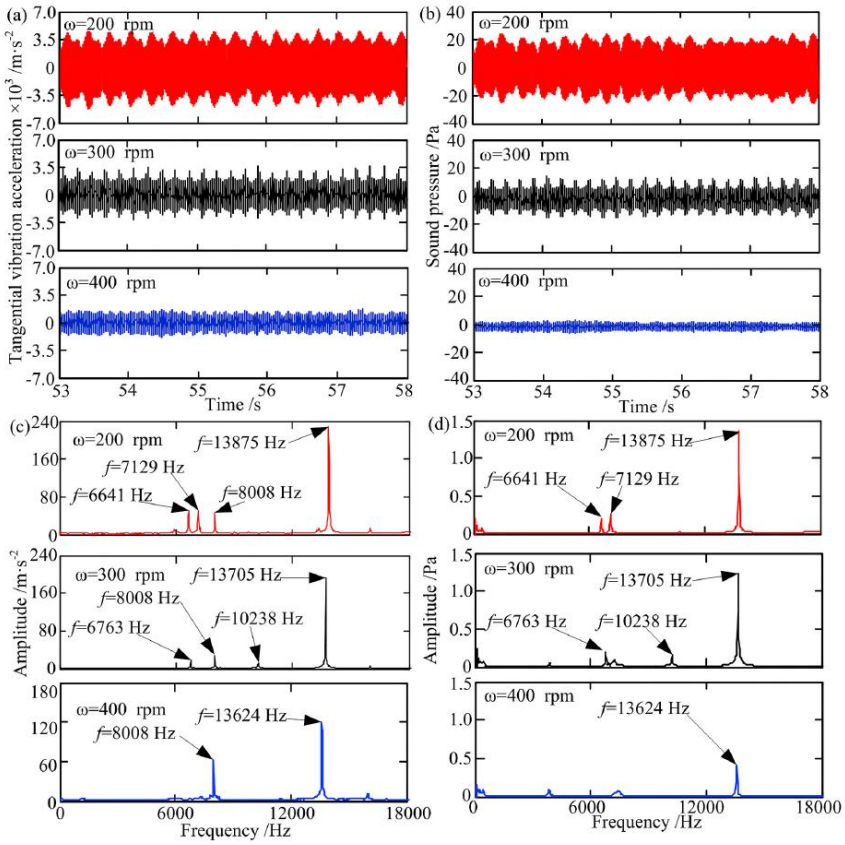

Fig. 3 Time-domain signals of the vibration (a) and sound pressure (b), and the vibration FFT (c) and sound pressure FFT (d) results at different brake disc rotation speeds

3.2 Frictional and wear analysis

Figure 4 (a) show the brake torque of the friction blocks during the test at the three rotation speeds of the braking disc (200 rpm, 300 rpm, and 400 rpm). The results show that the lower the brake disc rotation speed, the higher the brake torque was. The brake torque and its fluctuations were largest at a brake disc rotation speed of 200 rpm. The torque data in the stable squeal range of 53~58 s were converted into the friction coefficient to determine the correlation between the vibration and noise and the friction behaviour by using $\mu=T/(F*R)$ (where μ is the friction coefficient, T is the brake disc torque obtained from the test, F is the normal force, and R is the friction radius). The results are shown in the inset in Fig. 4 (a), and the average values of the coefficient are shown in Fig. 4 (b). The friction coefficient was the largest at the brake disc rotation speed of 200 rpm. Some studies have demonstrated that the instabilities of brake systems could be induced by a high friction coefficient [27, 50]. It is confirmed that the trend of the squeal vibration amplitude with respect to speed was due to a variation in the frictional response at the interface. A higher friction capacity resulted in higher tangential forces and consequently a higher power at the contact, feeding the unstable mode and thus increasing the vibration amplitude.

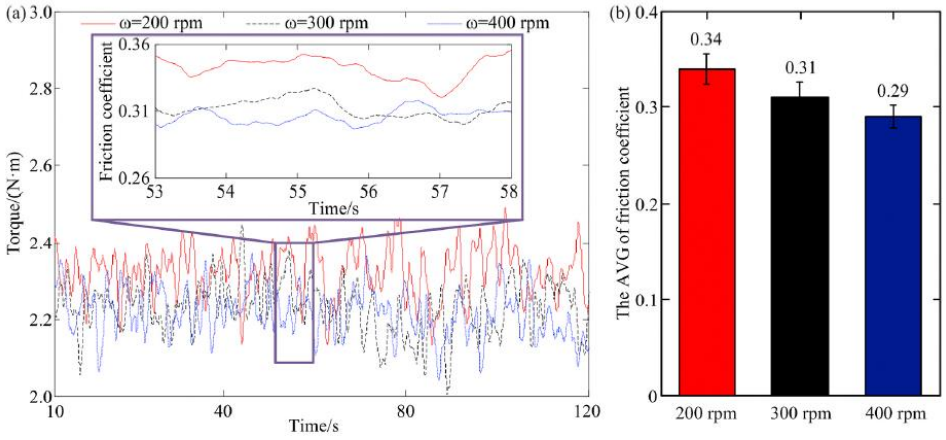

Fig. 4 Brake torque during the test (a) and mean value of the friction coefficient during the stable squeal stage of 53-58 s (b)

A pressure film was used to measure the pressure distribution at the contact interface when the brake disc was stopped after the friction test, and the contact pressure distribution of the friction block at different brake disc rotation speeds was obtained, as shown in Fig. 5 (a). Localised wear of the friction block can be clearly seen from the contact pressure distribution. A larger contact pressure distribution region means a lower contact pressure and a better contact performance under the static state, which indicates a better wear situation. On the other hand, the friction block exhibiting significant localised wear presents serious wear damage in the case of smaller contact pressure region.

All friction blocks exhibited an uneven distribution of the contact pressure. Areas of high contact pressure were located at the trailing edge of the friction block surfaces because the friction process resulted in localised wear, and the leading edge of the friction block was worn off to present a relatively low surface. These phenomena indicate that the surface-to-surface contact was nonuniform due to localised wear and component deformation, and a contact inclination angle existed between the friction block surface and brake disc surface. It is worth noting that the largest average pressure of 294.3 kPa occurred on the friction block surface at a brake disc rotation speed of 200 rpm, and the pressure decreased with an increase in the brake disc rotation speed. According to the equation:

$S = F/P$ (where P is the average contact pressure, F is the normal force, and S is the contact area), at the end of the test the friction block had the smallest contact area at 200 rpm and the largest contact area at 400 rpm, with an inverse trend in the contact pressure. The results indicate that the friction block presented significantly localised wear at a brake disc rotation speed of 200 rpm, which may result in serious wear damage on the friction block surface due to the larger contact stresses.

The surface temperature of the friction blocks after the test was monitored with a thermal imager, in order to analyse the contact area during the sliding process between the brake disc and friction block. As the rotation speed increased, the surface material generated plastic deformation due to the rise of temperature, and a larger amount of debris was accumulated in the wear area, which increased the contact area. The results (Fig. 5 (b)) show that the highest temperature did exhibit in the case with the highest speed. Within a certain period of time, the friction block rotated a longer distance at a larger brake disc rotation speed, producing more frictional work and heat. Therefore, the friction block with higher brake disc rotation speed exhibited higher temperature.

Additionally, a high-temperature area was located at the leading edge of the friction block, and the size of this area was related to the brake disc rotation speed. The higher the brake disc rotation speed, the larger the area of high temperature distribution was. This finding indicates that the contact area was larger at higher brake disc rotation speeds. The temperature field of the brake disc during the test (Fig. 6) confirmed these findings, e.g. the annular region in red or white colour (that was undergoing greater friction) widened with the increase of brake disc rotation speed. The observations highlighted that localised wear on the friction block surface was more pronounced at a brake disc rotation speed of 200 rpm.

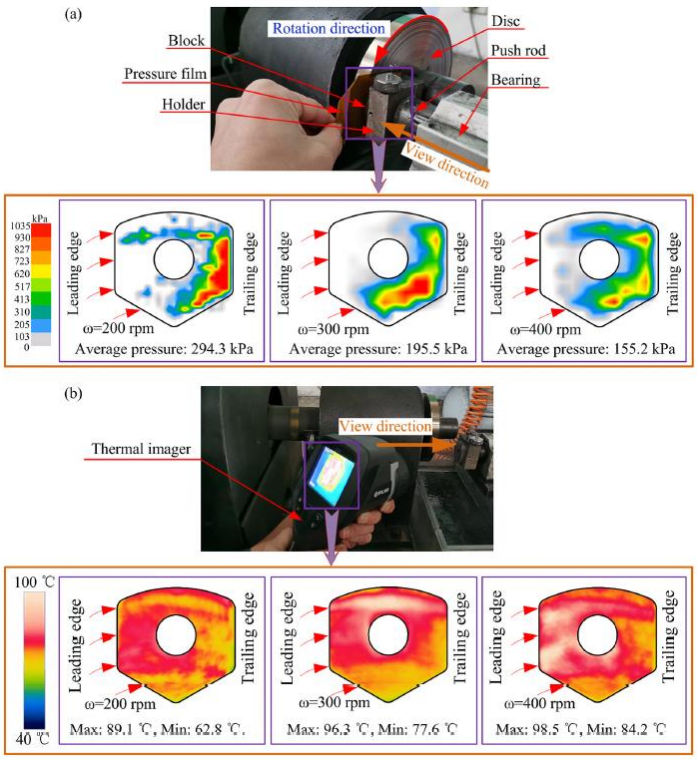

Fig. 5 Contact pressure (a) and surface temperature (b) of the friction block at the end of the test at different brake disc rotation speeds

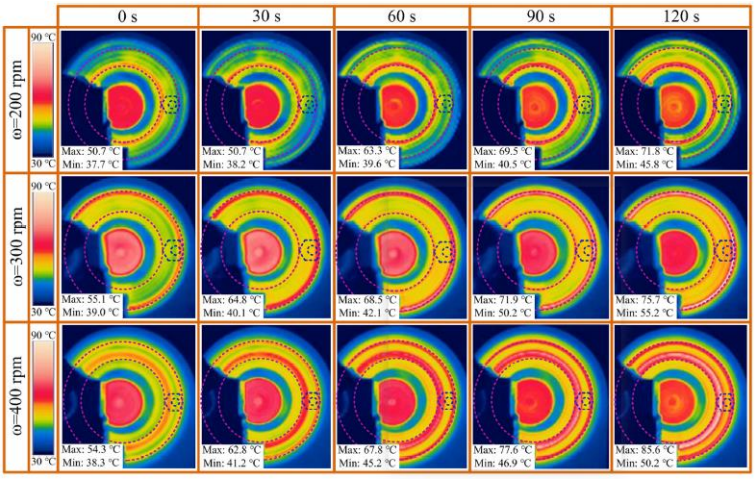

Fig. 6 Temperature field on the brake disc surface at different brake disc rotation speeds

Optical microscope images were obtained to analyse the wear characteristics of the friction block at the interface. Fig. 7 (a), (b), and (c) show optical microscope images and corresponding image segmentation results of the friction blocks' worn surfaces observed at brake disc speeds of 200 rpm, 300 rpm, and 400 rpm. The worn surfaces were characterized by two types of topographies. The first type of topography indicated by the bright yellow area was the metallic matrix exposed at the material surface; these areas represented plateaus with a relatively smooth surface. The second type of topography was represented by the brown areas, in which the material surface was covered by wear debris, which was the result of compacting and shearing. These surface areas were rubbed by large amounts of accumulated wear particles; thus, more exfoliation and ploughing were observed in these areas.

The friction blocks exhibited different wear characteristics at different rotation speeds during the braking process. The smaller zone of smooth contact plateaus was observed on the friction block surface at a brake disc rotation speed of 200 rpm, and the zone increased at speeds of 300 rpm and 400 rpm. Additionally, the Otsu threshold segmentation method was applied in the optical microscope images to quantitatively analyse the contact plateau. The image segmentation results further showed the characteristics of the contact plateaus on the worn surface of the friction block, and confirmed the above analysis. Additionally, the area of contact plateaus at the brake disc rotation speed of 200, 300 and 400 rpm were 299498, 357062 and 436773 μm^2, respectively. The results highlighted that the friction block had the smallest effective contact area at a brake disc rotation speed of 200 rpm.

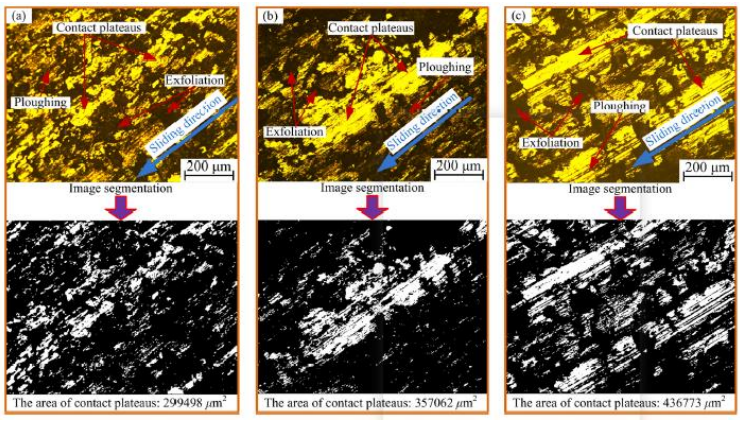

Fig. 7 Optical microscope images and corresponding image segmentation results of the friction block surface at different brake disc rotation speeds: (a) 200 rpm, (b) 300 rpm, (c) 400 rpm

The 3D topographies of the friction block surfaces at different brake disc rotation speeds were obtained using a white-light interferometer; the results are shown in Fig. 8. At a brake disc rotation speed of 200 rpm, the friction block exhibited an extremely rough worn surface (Fig. 8 (a)), and numerous exfoliations, deep furrows, and some contact plateaus were observed. With the increase in the brake disc rotation speed, the surface wear morphology of the friction block became slighter, and the contact plateaus on the worn surface became larger and smoother. The 3D topographies indicated that the higher the brake disc rotation speed, the larger the contact area was. This result was in good agreement with the optical microscope observations.

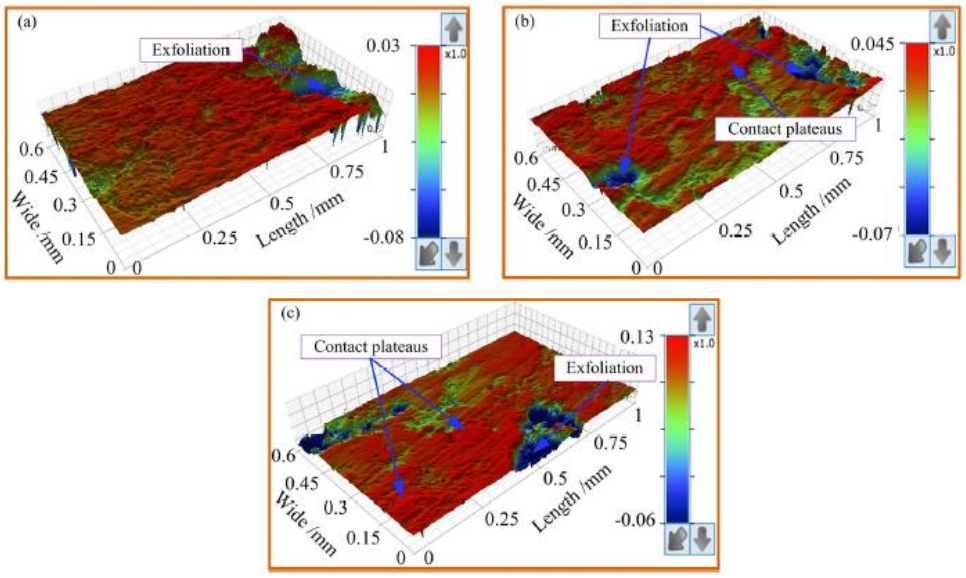

Fig. 8 3D topographies of the friction block surfaces at different brake disc rotation speeds: (a) 200 rpm, (b) 300 rpm, (c) 400 rpm

The vibration response and the contact behaviour at the three rotation speeds indicated that the contact behaviour was highly correlated with the vibration and noise levels of the brake systems. A relatively low brake disc rotation speed resulted in a higher friction coefficient, more substantial wear and more wear debris on the friction block surface, while numerous small and rough contact plateaus were observed. These contact plateaus bore most of the load and experienced the largest friction force at the contact interface [47, 57]. During the friction process, the area of greatest contact stress occurred on the plateaus; the highest contact stresses, due to the reduction of the effective contact area and increase in friction coefficient, led to a highest excitation of the system that responds with a higher vibration energy. As a result, vibration increased in the system. Therefore, at a brake disc rotation speed of 200 rpm, the friction block surface experienced higher friction and stronger wear, which resulted in higher vibration and sound pressure.

4 NUMERICAL SIMULATION ANALYSIS

The finite element (FE) methods CEA and TDA were executed in ABAQUS 6.14 to determine the dynamic evolutions of the contact behaviour and the vibration responses.

4.1 Establishment and validation of the finite element model

The finite element model of the brake dynamometer (Fig. 9 (a)) was a simplification of the dynamometer shown in Fig. 1. The model included six components: a brake disc sample, a friction block sample, a holder, an acceleration sensor, a linear bearing, and a push rod. Compared with other element types, C3D8R (a popular general-purpose 3-dimensional linear brick element with reduced integration in ABAQUS) can efficiently reduce computational time and ensure higher accuracy. Therefore, the FE model in this manuscript was discretised with C3D8 brick elements. The computational efficiency and results of the model could be dramatically affected by the mesh size. A coarse grid may lead to unreliable results, while a too dense grid may lead to a low computing efficiency [22]. Before carrying out the transient analysis, the contact stresses have been computed using a series of increasingly dense grids until the obtained stresses converged. Ultimately, the maximum element sizes of the FE model were set to: 4 mm for brake disc, 1.2 mm for friction block, 1.5 mm for sensor, 2 mm for holder, 4 mm for bearing and push rod, resulting in 22057 elements and 63829 nodes for the whole model.

The reference coordinate system included the tangential (X), radial (Y), and normal (Z) directions. The boundary conditions were set according to the real loading conditions. As shown in Fig. 9 (b), a fixed constraint was applied to the underside of the linear bearing, and the brake pressure was loaded vertically on the end face of the push rod. The brake disc sample had a speed boundary condition, and the rotation was around the normal (Z) axis; the surface of the brake disc was taken as the master surface and the friction block surface as the slave surface. The connections between the components are shown in Table 4. The material parameters of all components are shown in Table 3.

Table 4 Connections between the components of the finite element model

Number	Interconnected parts	Real connection	Model method in ABAQUS
1	Disc-block	Contact	Surface-to-Surface Contact
2	Block-holder	Tie	Tie
3	Sensor-holder	Tie	Tie
4	Push rod-holder	Tie	Tie
5	Pushrod-bearing	Hinge	Surface-to-Surface Contact

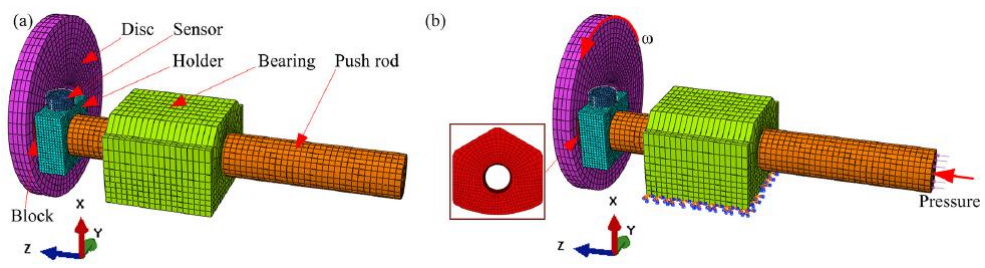

Fig. 9 Finite element model (a) and boundary conditions (b) of the brake dynamometer

CEA is commonly used to verify the reliability of the finite element model and estimate the stability of the brake system by comparing the frequency of the unstable modes of vibrations with the dominant frequency of the squeal obtained from the experimental test. Additionally, the unstable modal shapes of the brake system, brake disc, and friction block can be observed. Unstable vibration of the brake system can occur if the damping ratio of the eigenvalue is negative; otherwise, the system remains in a stable state. In this study, the friction coefficients of the disc/block and pushrod/bearing interface were in the range of 0.1-0.6 and 0.1, respectively. The brake pressure and the brake disc rotation speed were set to 0.269 MPa (amounts to a brake force of 190 N) and 200 rpm, respectively.

Figure 10 (a) shows the evolution of the frequency and damping ratio with the increase in the friction coefficient for the 32nd and 33rd modes of the brake system. The results indicate that when the friction coefficient reached the critical value (μ=0.187), mode coupling of the two modes occurred at a frequency of 13427 Hz, indicating that the system reached an unstable state. The mode shapes of the brake system (Fig. 10 (b)), the brake disc and the friction block (Fig. 10 (c)) show that the brake disc exhibited mainly normal (Z-direction) vibration, and the friction block exhibited tangential (X-direction) vibration. Moreover, the unstable vibration frequency determined by CEA was quite close to the dominant frequency (13875 Hz) of the squeal noise obtained from the experiments at 200 rpm, and the relative error between the results was only 3.2 %. Thus, it can be concluded that the finite element model provided an excellent indication of the dynamic characteristics of the brake system.

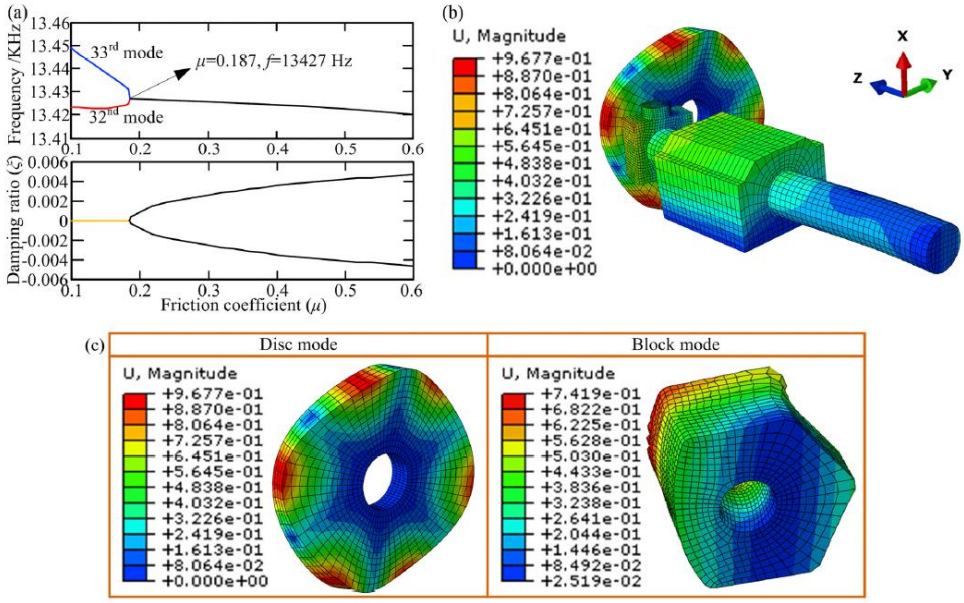

Fig. 10 Frequency and damping ratio (a) and the corresponding mode shape of the brake system (b) and the brake disc and friction block (c) due to mode coupling

4.2 Transient dynamic analysis (TDA) of the brake system

TDA was performed using ABAQUS/Explicit solver. It is worth noting that thermal effect is not negligible in the finite element analysis if the temperature of the braking interface is too high [58]. However, from Fig. 5 and Fig. 6, it was found that the measured temperature was too low to significantly affect the mechanical properties

of the bulk of the friction materials in these brake tests. Thus, the thermal effect was not considered in the FE model.

The dynamic response, including vibration acceleration, velocity, and displacement and the interface contact behaviour, including the friction force and contact area, were obtained. In the TDA, the connections between the components and the boundary conditions of the brake system were set to be the same as in the CEA. The setting of the simulation, i.e., the normal load (brake pressure) and the brake disc rotation speed in the time-domain are shown in Fig. 11. The brake pressure increased gradually from 0 to 0.269 MPa during the period of 0.01 s and then kept constant. After that, the brake disc rotation speed gradually increased from 0 to the experimental speed. In addition, the friction coefficients at the disc/block interface were selected according to the experiment results. i.e. 0.34, 0.31 and 0.29 (corresponding to the brake disc rotation speed of 200 rpm, 300 rpm and 400 rpm).

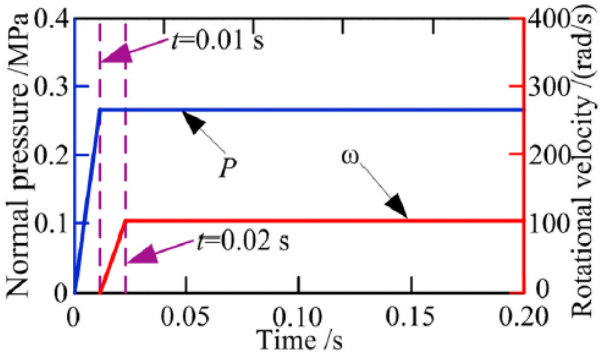

Fig. 11 Curves of applied normal pressure P and the brake disc rotation speed ω in time-domain

4.2.1 Interfacial friction force

It has been reported that the interfacial friction force is strongly correlated to the vibration intensity of the brake system [34-37]. Therefore, the friction force of the disc/block interface was analysed using TDA at different brake disc rotation speeds; the results are shown in Fig. 12. At all the three rotation speeds, the friction force suddenly increased at 0.01 s and then exhibited strong oscillation with steady amplitude. Thus, the friction force varied with time even though the friction coefficient of the brake interface was constant in the finite element model. Introducing friction coefficients that depended on disc rotation speeds into the FE model to obtain the corresponding friction forces, it was found that the average (AVG) oscillation amplitude and the standard deviation (SD) of friction force were largest at 200 rpm, followed by those at 300 rpm and 400 rpm. The vibration acceleration and sound pressure intensity exhibited the same trends (as shown in Fig. 3) with changes in the brake disc rotation speed.

The FFT analysis results of the friction force are presented in Fig. 12 (b). The friction forces at the different speeds all exhibited a dominant frequency signal with high amplitude, namely, 13957 Hz, 13935 Hz, and 13896 Hz, respectively; these situations were consistent with the vibration frequency of the brake system shown in Fig. 3, considering that the relative errors are only 0.59%, 1.68%, and 1.99%, respectively. Simultaneously, it was found that the energy of the dominant frequency decreased with the increase in the brake disc rotation speed, which was also consistent with the trends of the vibration characteristics. These observations confirm that the

oscillation of the friction force was a key factor that affects the unstable vibration of the brake system.

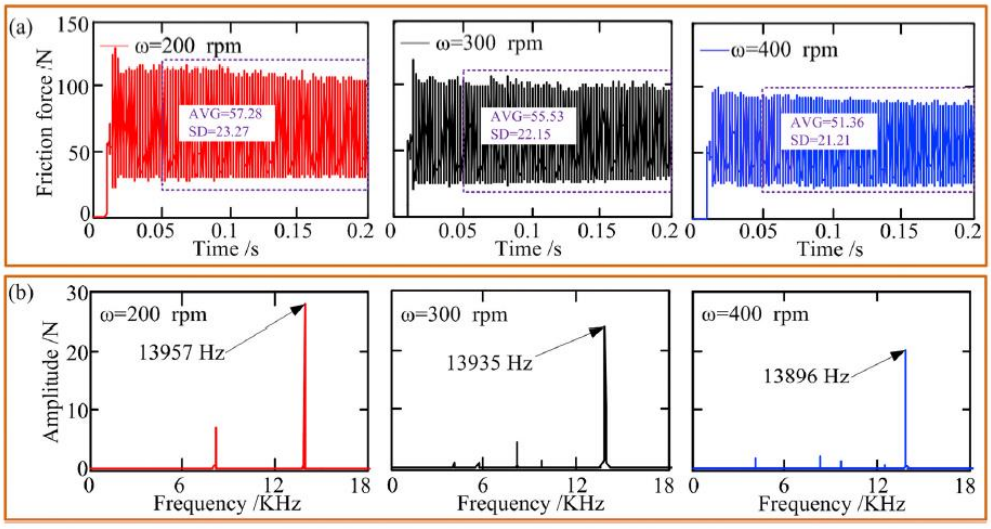

Fig. 12 TDA results of the friction force (a) and FFT analysis (b) at the three test speeds

4.2.2 Contact inclination angle

The results demonstrated that the interfacial friction force induced high-frequency vibrations at the friction interface of the brake system, and different vibration characteristics were observed at different brake disc rotation speeds. The contact inclination angle was another factor that influences the vibration response. The friction block would move along the sliding direction as a result of the interface friction force, causing deformation in the friction block and thus creating the contact inclination angle. The brake tests were not long and thus wear was slight and could not affect the inclination angle.

The displacements of several nodes on the friction block were analysed to determine the change in the contact inclination angle at different brake disc rotation speeds. The positions of nodes N-1, N-2, N-3, and N-4 on the friction block are shown in Fig. 13. Their displacements were determined using the coordinate system exhibited in Fig. 13, in which the X-, Y-, and Z-axes represented the tangential, radial, and normal directions, respectively. Nodes N-1, N-2, N-3, and N-4 were located on the Z-axis, and their displacements in the tangential direction (X-axis) during the dynamic instability period at different brake disc rotation speeds are shown in Fig. 14. The results show that all node displacements had negative values, which demonstrated that the brake disc sheared the friction block in the opposite direction of the X-axis as a result of the interface friction force. Moreover, the oscillation magnitudes of displacements of all these nodes exhibited decreasing trends with the increase in the brake disc rotation speed. This finding indicated that the friction block suffered the strongest vibration at the brake disc rotation speed of 200 rpm; these results were consistent with the experimental results.

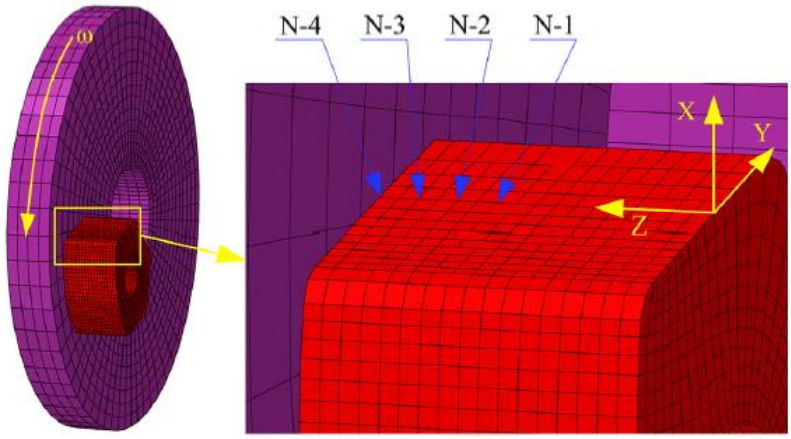

Fig. 13 The node positions N-1, N-2, N-3, and N-4 on the friction block

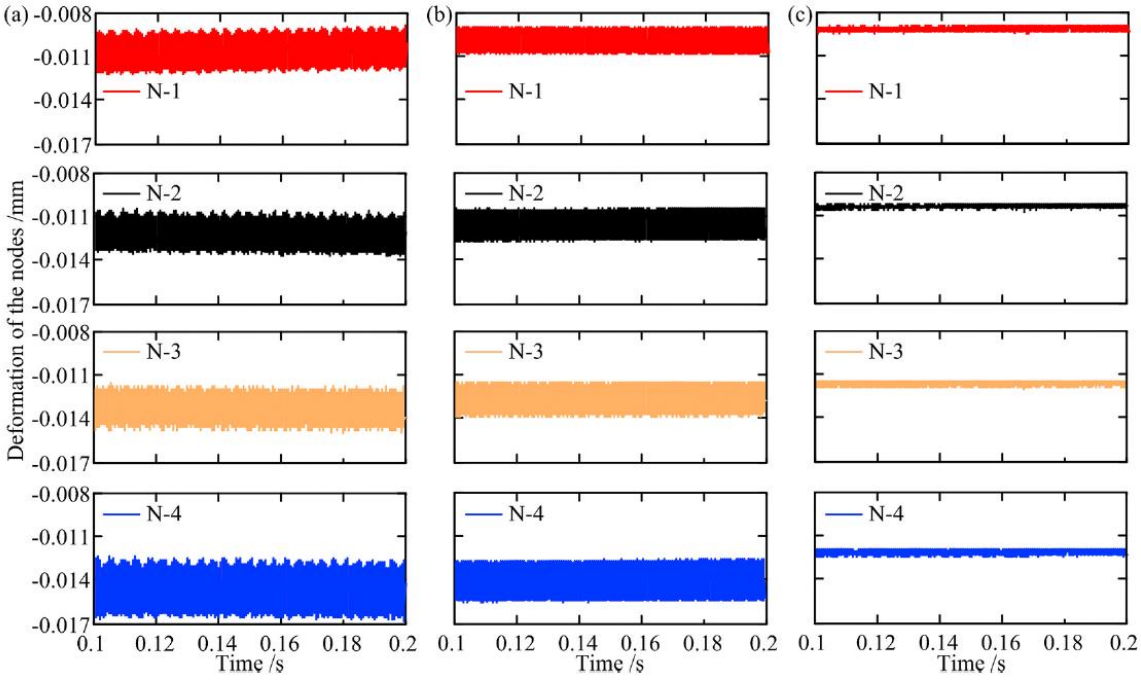

Fig. 14 Displacement of nodes N-1, N-2, N-3, and N-4 in the tangential direction at different brake disc rotation speeds of 200 rpm (a), 300 rpm (b), and 400 rpm (c)

The average displacements (over the duration of 0.1~0.2 s) of the nodes were calculated and fitted to a straight line, as shown in Fig. 15. The displacement gradually increased from N-1 to N-4 for all the three rotation speeds. The angle between the fitted straight line and the normal direction (Z-axis) was defined as the contact inclination angle (θ) between the brake disc surface and friction block surface. It was found that the contact inclination angle (magnitude) decreased with the increase in the brake disc rotation speed. The results also showed that the localised wear of the friction block surface was more severe at the speed of 200 rpm; the numerical results on the inclination angle were coherent with the experimental observations, as shown in Fig. 7 and Fig. 8.

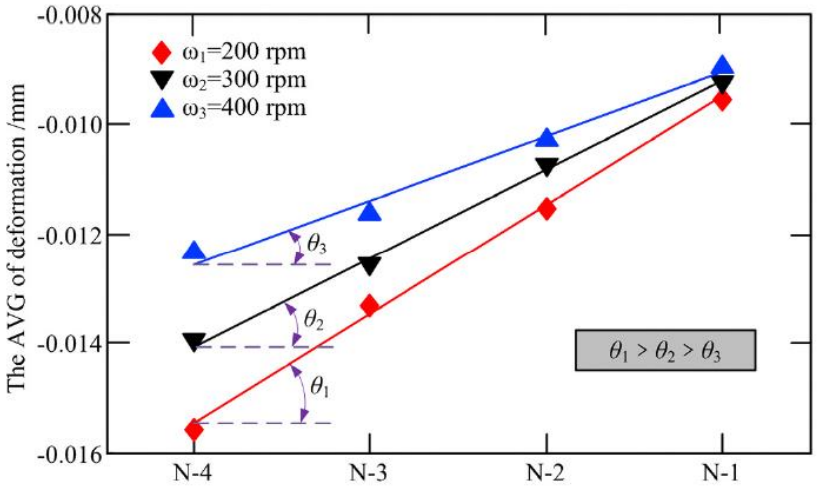

Fig. 15 Average displacement of nodes N-1, N-2, N-3, and N-4 in the tangential direction

As shown in Fig. 16 (a), the friction process resulted in imperfect contact between the surfaces due to the asymmetric loading; the larger the contact inclination angle, the more uneven the contact and the more likely the occurrence of concentrated stress were. Figure 16 (b) exhibits the distribution of contact pressure of the friction block surfaces, indicating that a region of concentrated contact pressure occurred at the leading edge of the friction block surface at all the rotation speeds; the contact pressure became more uniform with the increase in the brake disc rotation speed. It has been reported that a more evenly distributed contact pressure distribution on the friction block surface resulted in lower vibration and sound pressure of the brake system [27]. In this study, the brake system exhibited the strongest vibration at the brake disc rotation speed of 200 rpm whereas the lowest vibration intensity occurred at a speed of 400 rpm.

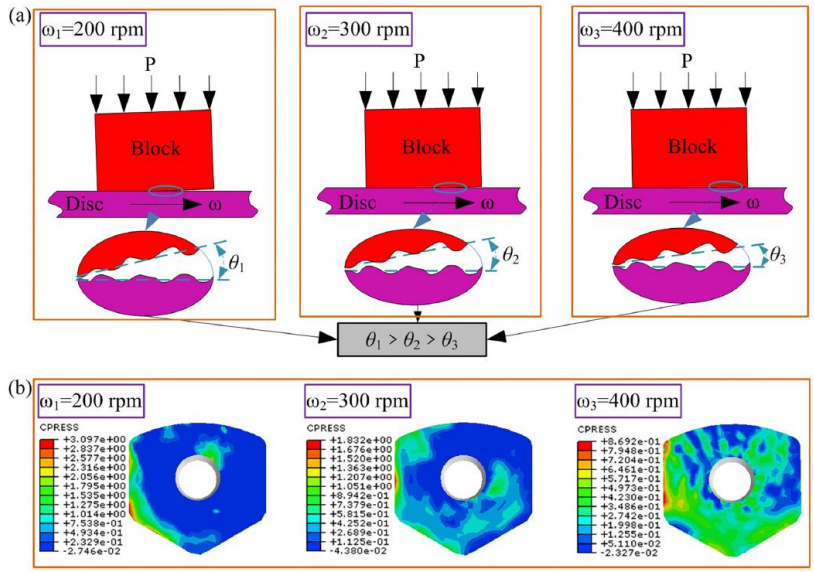

Fig. 16 Schematic diagram of the contact inclination angle at different brake disc rotation speeds of 200, 300, and 400 rpm (a) and the contact stress on the friction block surface (b)

4.2.3 Contact area and contact pressure

The time-domain variations of the contact area at different brake disc rotation speeds are shown in Fig. 17 (a). The results show that the contact area of the friction block suddenly decreased after rotating the brake disc; subsequently, oscillations with a steady amplitude occurred at all the three speeds. Thus, the contact area exhibited a time-varying evolution and the friction interface was in incomplete contact during the friction process. The AVG and SD of the contact area during a steady period (0.05~0.2 s) were 384.14 mm^2 and 90.87 mm^2, respectively (shown in Fig. 17 (a)). These values were lowest at 200 rpm, followed by 300 and 400 rpm. The results indicated that the contact area of the friction block surfaces increased with the increase in the brake disc rotation speed; the results were consistent with the contact pressure results shown in Fig. 5 (a).

The results of the time-frequency analysis are depicted in Fig. 17 (b). The dominant frequencies of the contact area variation at the brake disc rotation speeds of 200, 300, and 400 rpm were 13957 Hz, 13935 Hz, and 13896 Hz, respectively; these values were similar to the dominant frequencies of the friction force (Fig. 12) and vibration (Fig. 3). In addition, the energy of the high-frequency component of the contact area was the highest at the brake disc rotation speed of 400 rpm, exhibiting the largest fluctuation of contact area in this speed condition. This result indicated that there was a bigger partial contact loss between the two sliding surfaces at the highest brake disc rotation speed observed in this experimental study. During the friction process, the amplification of the friction-induced vibration energy generated by the brake interface was limited by the contact separation [59]. Thus, the brake system exhibited the lowest vibration energy (as shown in Fig. 3) at the brake disc rotation speed of 400 rpm.

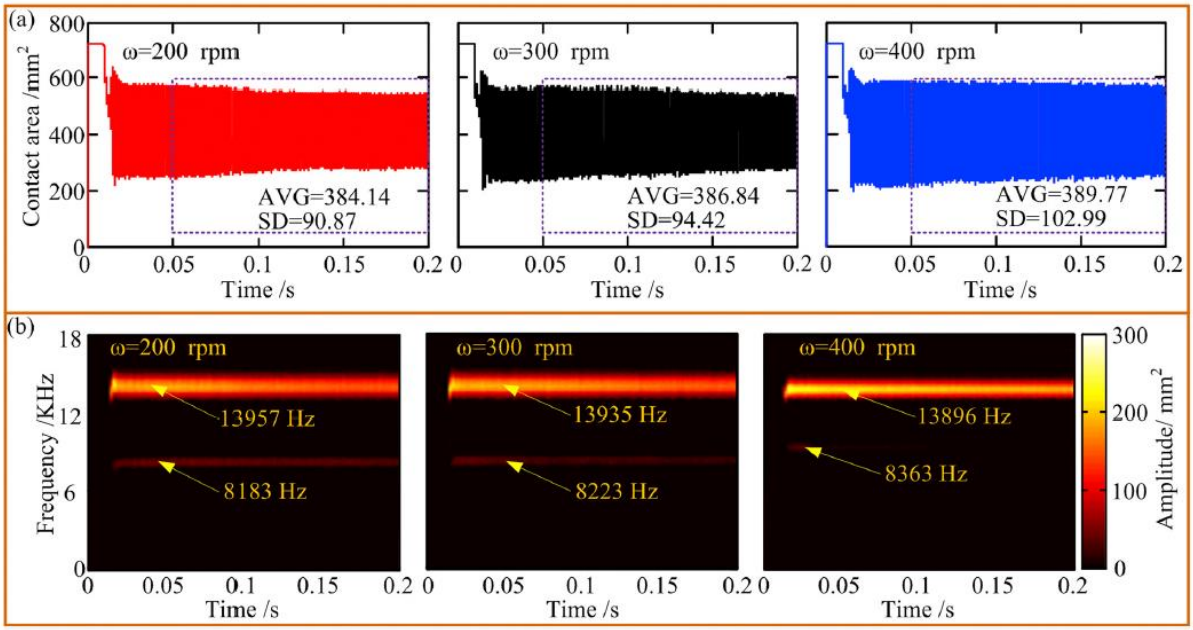

Fig. 17 Time-domain signal (a) and time-frequency analysis (b) of the interface contact area at different brake disc speeds

The interface contact area and the contact pressure were investigated at different times during a squeal

occurrence interval of 0.0004 s (Fig. 18). The contact area of the friction blocks at all the three brake disc rotation speeds showed continuous oscillations with a relatively large fluctuation range of more than 200 mm^2. The contact pressure distributions of the friction block surfaces corresponding to the largest amplitude of the contact area in several oscillation periods were shown. Although the distribution of the contact pressure changed constantly, larger contact pressure occurred at the leading edge of the friction block surface. Moreover, it was observed that the higher the brake disc rotation speed, the more uniform the distribution of contact stress was. Moreover, comparatively, the maximum contact pressure on the friction block surface was lowest at a speed of 400 rpm than for the other two speed conditions.

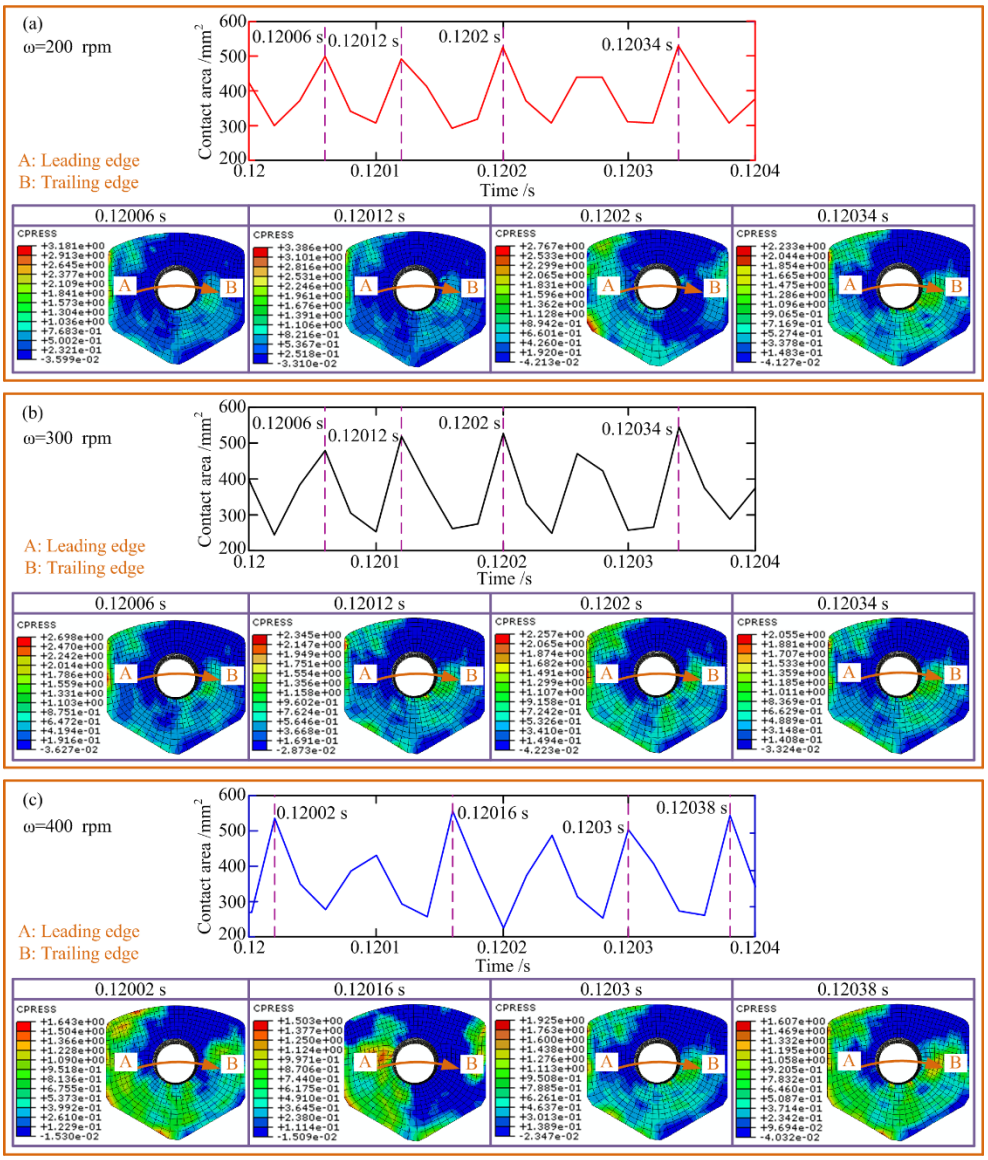

Fig. 18 Interface contact area and the contact pressure of the friction blocks at different times: (a) 200 rpm, (b) 300 rpm, (c) 400 rpm (the arrow points to the direction of the brake disc velocity)

4.2.4 Discussion on the relationship between the interface contact behaviour and the vibration response

The relationship between the interface contact behaviour and vibration response of the brake system is

illustrated in Fig. 19. In this study, the block surfaces exhibited different wear characteristics at different brake disc rotation speeds. The test results show that the contact interface displayed a higher wear debris accumulation, more ploughing and exfoliations, and rougher contact plateaus at a lower brake disc rotation speed (Fig. 7 and Fig. 8). This type of wear resulted in a higher friction force and friction coefficient (Fig. 4). In addition, at a lower rotation speed of brake disc, at the end of braking test when disc rotation was stopped (Fig. 5 (a)), the contact pressure distribution of the friction block was found to be more concentrated and the average value of contact pressure was larger and the trailing edge bore more contact pressure. Therefore, a larger contact inclination angle appeared between the brake disc and the friction block during the experiment. From the contact pressure of the block at different brake disc rotation speeds (Fig. 5 (a)) after the disc rotation was stopped, it can be concluded that during the brake test the larger the speed of brake disc, the smaller the inclination angle resulted.

The numerical results show that the brake disc, rubbing against the block with the friction force, deformed the friction block and created a contact inclination angle between the brake disc surface and the block surface. Thus, the FE results further confirmed that the inclination angle existed during the rubbing of brake disc and friction block. The larger the friction force, the larger the contact inclination angle was (Fig. 15), resulting in uneven contact between the brake disc and the block; in this case (Fig. 16), the effective contact area of the friction block was smaller than the apparent contact area of the block (Fig. 17).

Moreover, the contact pressure distribution on the block surface was strongly correlated with the contact area of the block; the average contact pressure was smaller for a larger contact area (Fig. 18). In contrast, a smaller contact area resulted in a region of higher concentrated contact pressure at the leading edge of the block, which explained the increase in the surface degradations (ploughing and exfoliations) discussed above (in section 3.2). It was speculated that the higher the contact pressure, and the differences in the rheological and physiochemical responses of the interface, with the imposed speed, led to an increase in the average friction coefficient. This condition caused stronger vibration and higher sound pressure.

There was an inherent relationship between the vibration response and the surface contact behaviour of the brake system [55]. The rheological and physiochemical response of the interface generated the stronger and complex vibration response, which had been discussed before. Meanwhile, the vibration response may also affect the complex surface contact behaviour, such as oxidation and thermal effects, which occur at the contact interface [32]. In [60], it was shown how the contact plateaus of friction blocks bore most of the normal load and experienced the largest friction stresses at the contact interface; the tangential vibrations may create more ploughing and shearing in the friction process, while the normal vibration mainly caused impact on the contact interface, resulting in the peeling of the materials on the contact surface and peeling pits of different sizes. In addition, the overall surface wear increased as the vibration of the system increased, indicating the complex interaction of the contact behaviours.

The contact inclination angle between the brake disc and the block was found to be a crucial factor affecting the vibration characteristics of the brake system. In a high-speed train brake system, it is not only necessary to reduce vibration and the noise intensity of the braking system, but also to ensure an appropriate friction and wear of the contact interface to maintain safe and reliable operation of trains. Therefore, effective solutions should be taken to reduce the contact inclination angle of the block and spread the interface contact pressure to avoid regions of concentrated contact pressure.

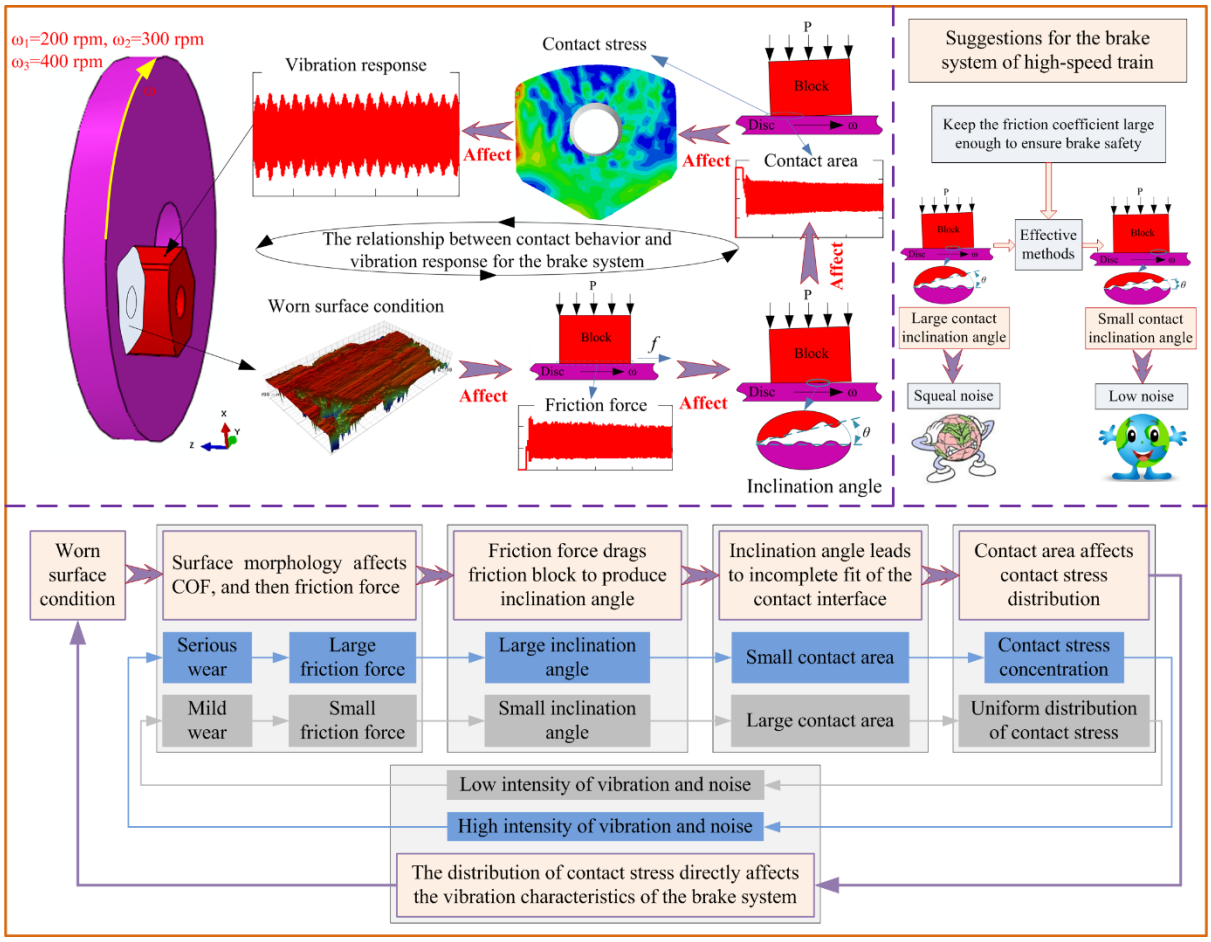

Fig. 19 Schematic diagram of the relationship between the contact behaviour and vibration response of the braking system

4.3 Two-degree-of freedom friction-induced model with contact inclination angle

To further investigate the mechanism of unstable FIV, the FEA model (Fig. 9) was simplified as a rigid conveyor belt running at a constant speed and a mass block sliding on it, simulating the FIV generated at the interface between the friction block and brake disc. The stiffness matrix that is originally symmetric becomes asymmetric when friction is involved, which can produce complex eigenvalues of the equation having a positive real part, and the system then can be regarded as unstable.

Therefore, a two-degree-of-freedom (DOF) friction-induced model was established, based on the mode-coupling theory [38], to further explore the relationship between the contact behaviour and the vibration response; the model is shown in Fig. 20. It is worth noting that the model was used to capture the essential characteristics of the brake system rather than reproducing the experimental results. The interfacial factors, including the contact inclination angle (θ) (between the mass (m) and the belt) and the friction coefficient (μ) were considered in this model to study the stability and vibration response of the brake system. The normal force (F_n) was loaded onto the mass (m) so that it could contact the rigid moving belt in this numerical model. The belt moved at a constant velocity (v). The constraint on mass (m) was depicted by two linear oblique springs (k_1 and k_2), and the angles

between the two linear springs and the upper surface of the mass (m) were 135° and 45°, respectively. The normal and tangential contact stiffness between the mass (m) and the rigid moving belt were replaced by the two linear oblique springs (k_n and k_t).

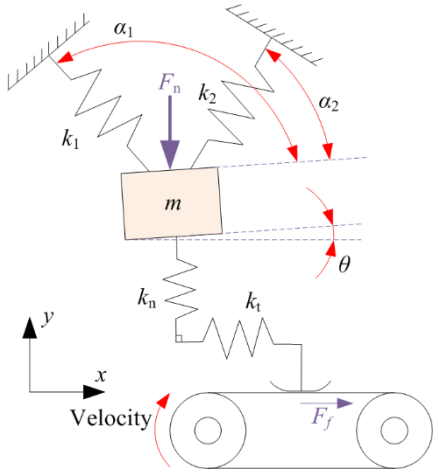

Fig. 20 A two-DOF friction-induced model that considers the contact inclination angle

In this model, the friction coefficient (μ) between the mass and the rigid moving belt was constant, and the dynamic equation of the two-DOF model shown in Fig. 20 was defined as:

$$\begin{bmatrix} m & 0 \\ 0 & m \end{bmatrix}\begin{bmatrix} \ddot{x} \\ \ddot{y} \end{bmatrix}+\begin{bmatrix} K_{11} & K_{12} \\ K_{21} & K_{22} \end{bmatrix}\begin{bmatrix} x \\ y \end{bmatrix}=\begin{bmatrix} F_f \\ F_n \end{bmatrix} \tag{1}$$

The parameters of the stiffness matrix in Eq. (1) were:

$$K_{11}=k_1\cos^2(\alpha_1+\theta)+k_2\cos^2(\alpha_2+\theta)+k_t$$

$$K_{12}=K_{21}=k_1\sin(\alpha_1+\theta)\cos(\alpha_1+\theta)+k_2\sin(\alpha_2+\theta)\cos(\alpha_2+\theta)$$

$$K_{22}=k_1\sin^2(\alpha_1+\theta)+k_2\sin^2(\alpha_2+\theta)+k_n$$

To simplify the dynamic model, the horizontal motion of m was assumed to be in pure slip regime and the friction force was approximated as: $F_f=\mu k_n y$.

To investigate the stability of the dynamic system, Eq. (1) was converted to:

$$\begin{bmatrix} m & 0 \\ 0 & m \end{bmatrix}\begin{bmatrix} \ddot{x} \\ \ddot{y} \end{bmatrix}+\begin{bmatrix} K_{11} & K_{12}+\mu k_n \\ K_{21} & K_{22} \end{bmatrix}\begin{bmatrix} x \\ y \end{bmatrix}=\begin{bmatrix} 0 \\ 0 \end{bmatrix} \tag{2}$$

Introducing $P_1=x$, $P_2=y$, $P_3=\dot{x}$, and $P_4=\dot{y}$ so that Eq. (2) could be rewritten in the following matrix form:

$$\begin{bmatrix} \dot{P}_1 \\ \dot{P}_2 \\ \dot{P}_3 \\ \dot{P}_4 \end{bmatrix} = \begin{bmatrix} 0 & 0 & 1 & 0 \\ 0 & 0 & 0 & 1 \\ \frac{-K_{11}}{m} & \frac{-K_{12}+\mu k_n}{m} & 0 & 0 \\ \frac{-K_{21}}{m} & \frac{K_{22}}{m} & 0 & 0 \end{bmatrix} \begin{bmatrix} P_1 \\ P_2 \\ P_3 \\ P_4 \end{bmatrix} \tag{3}$$

Therefore, the Jacobian matrix (J) of this model was written as:

$$J = \begin{bmatrix} 0 & 0 & 1 & 0 \\ 0 & 0 & 0 & 1 \\ \frac{-K_{11}}{m} & \frac{-K_{12}+\mu k_n}{m} & 0 & 0 \\ \frac{-K_{21}}{m} & \frac{K_{22}}{m} & 0 & 0 \end{bmatrix} \tag{4}$$

The system was stable if the real parts of all the eigenvalues of the system were smaller than 0 (Re(s)≤0). Conversely, if the real part of any eigenvalue exceeded 0 (Re(s)>0), the system was unstable. The system parameters in the following numerical analysis were: m=1 kg, k_1=k_2=k_n=k_t=10^5 N/m, α_1=135°, α_2=45°, F_n=1 N. The eigenvalues of J were obtained by solving Eq. (4).

Figure 21 shows the results regarding the contact inclination angle and friction coefficient; the results were used to determine the stability of the brake system. If the contact inclination angle or the friction coefficient were relatively small, the brake system exhibited no modal coupling and was stable. The brake system gradually became unstable with the increase in the contact inclination angle and the friction coefficient, exhibiting vibration energy accumulation.

The experimental results indicated that the contact inclination angle had a positive correlation with the friction coefficient. In fact, the increasing in the inclination angle increased the local pressure (smaller contact surface), modifying the interface rheology and leading to a higher average friction coefficient. Then, a linear relationship was assumed between inclination angle and friction coefficient in this two-DOF model. Four configurations (P_1 (μ =0.1, θ =0.05°), P_2 (μ =0.2, θ =0.1°), P_3 (μ =0.3, θ =0.15°), and P_4 (μ =0.4, θ =0.2°)) (Fig. 21 (c)) were selected to analyse the vibration response. It was found that P_1, P_2, and P_3 were in the stable state of the system (no mode coupling), whereas P_4 was in an unstable state (mode coupling); the vibration accelerations in the tangential and normal directions were calculated by solving the system's dynamic equation (Eq. (1)), as shown in Fig. 22. The results showed that the tangential and normal vibration accelerations increased with the increase in the friction coefficients and contact inclination angle. When the brake system exhibited mode coupling and became unstable, the vibration accelerations increased sharply in both directions. The relationship between the contact behaviour and the vibration response obtained from the two-DOF friction-induced model was consistent with the findings of the experiments and the finite element analysis. These results allowed for assuming that both the contact inclination angle and friction coefficient could have a significant impact on the stability and vibration intensity of the brake system.

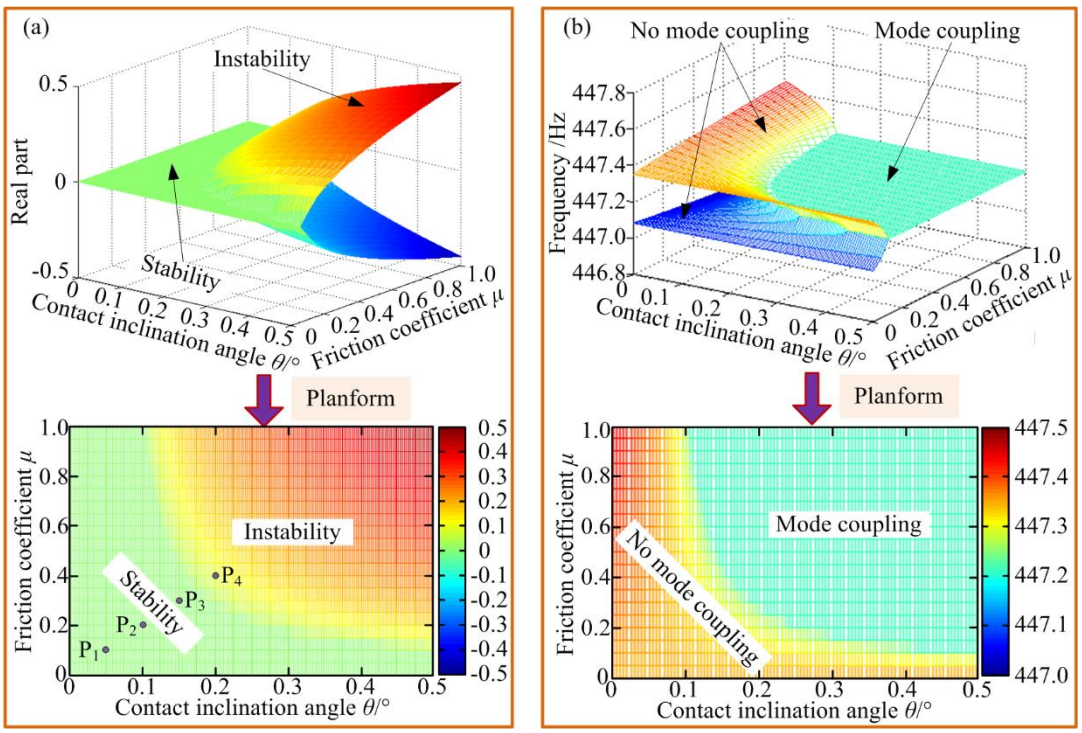

Fig. 21 Real part (a) and frequency (b) of the eigenvalue of the brake system

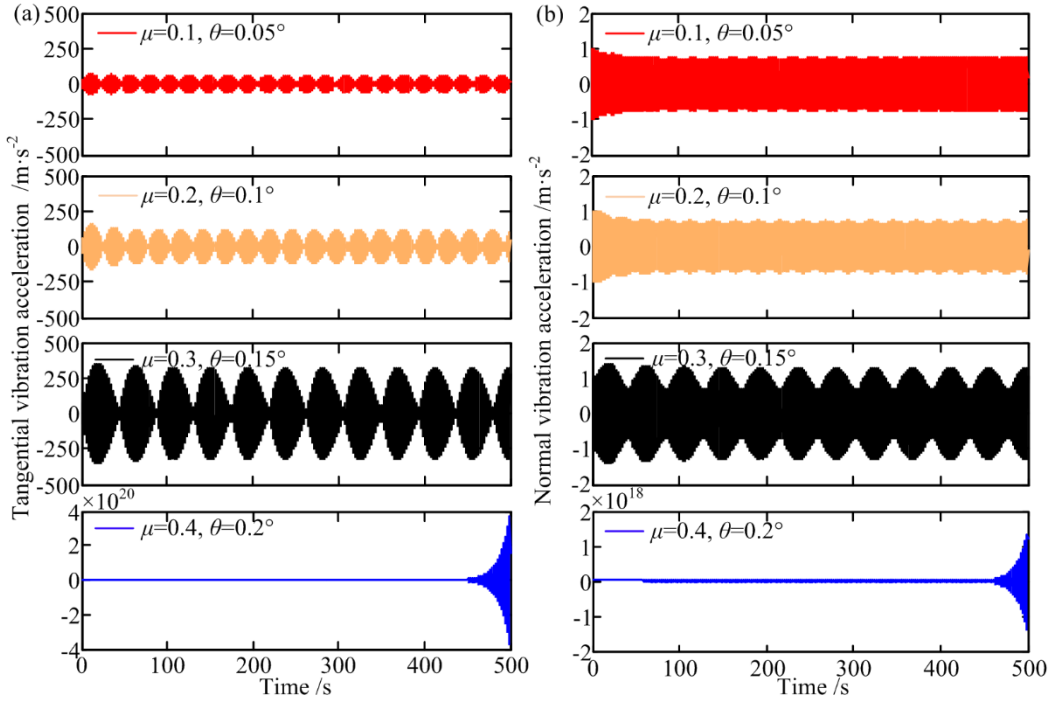

Fig. 22 Tangential (a) and normal vibration acceleration (b) of the brake system for different friction coefficients and contact inclination angles

5 CONCLUSIONS

In this work, the relationship between the contact behaviour of the friction interface and the vibration

response of a brake system of a high-speed train was investigated experimentally and numerically. The main conclusions drawn from this investigation are as follows:

(1) The experimental results indicated that the brake interface exhibited different vibration responses and contact behaviours at different brake disc rotation speeds. The strongest vibration response and the highest sound pressure level of the brake system occurred at a relatively low brake disc rotation speed. In that case, the friction block exhibited higher friction and severe localised wear and a rough wear surface.

(2) The friction blocks showed uneven contact pressure distribution during the test at the three rotation speeds of the braking disc. Areas of concentrated contact pressure were located at the trailing edge of the friction block surfaces after the tests, indicating that the friction process resulted in localised wear; a contact inclination angle between the friction block surface and the brake disc surface was observed. Additionally, the surface temperature distribution of the friction blocks further confirmed these results.

(3) The finite element analysis showed that the high-frequency squeal noise generated by the brake interface occurred during the selected experimental conditions, and the brake system became increasingly unstable with the increase in the friction coefficient. Additionally, the contact inclination angle between the friction block surface and the brake disc surface affected the contact behaviour, including the contact area and contact pressure distribution; this, in turn, affected the stability and vibration response of the brake system. The brake system became increasingly unstable with the increase in the friction coefficient and thus the contact inclination angle, thereby exhibiting higher vibration energy accumulation.

(4) A two-DOF friction-induced model was provided to describe the basic characteristics and determine the stability of the brake system. The numerical analysis results confirmed that both the friction coefficient and the contact inclination angle had a significant influence on the stability of the brake system.

The results of this study highlighted the correlation between the tribological behaviour of the brake interface and the vibrational response of the brake system, and the contact inclination angle between the brake disc and the friction block was found to be a crucial factor, affecting the vibration characteristics of the braking system. Therefore, effective solutions (e.g. adding a suitable elastic damping element to the back of the friction block) should be taken to reduce the contact inclination angle of the friction block and spread the interface contact stress to avoid regions of concentrated contact stress.

ACKNOWLEDGMENTS

The authors are grateful for the financial support of the National Natural Science Foundation of China (No. 51822508, No. 11672052), and Sichuan Province Science and Technology Support Program (No. 2020JDTD0012).

REFERENCES

[1] Chiello O, Sinou J-J, Vincent N, Roches G V D, Cocheteux F, Bellaj S, et al. Squeal noise generated by railway disc brakes: Experiments and stability computations on large industrial models. Journal of the Acoustical Society of America. 2013;133:1-9.

[2] Heckmann A, Kurzeck B, Carrarini A, Guenther F, Schroeder-Bodenstein K. Influences on nonlinear judder vibrations of railway brakes. Vehicle System Dynamics. 2010;48:659-674.

[3] Tirovic M. Energy thrift and improved performance achieved through novel railway brake discs. Applied Energy. 2009;86:317-324.

[4] Grzes P, Oliferuk W, Adamowicz A, Kochanowski K, Wasilewski P, Yevtushenko AA. The numerical-experimental scheme for the analysis of temperature field in a pad-disc braking system of a railway vehicle at single braking. International Communications in Heat and Mass Transfer. 2016;75:1-6.

[5] Tang B, Mo JL, Zhang X, Zhang Q, Zhu MH, Zhou ZR. Experimental investigation of the squeal characteristics in railway disc brakes. Proceedings of the Institution of Mechanical Engineers Part J-Journal of Engineering Tribology. 2018;232:1437-1449.

[6] Lazim ARM, Kchaou M, Hamid MKA, Abu Bakar AR. Squealing characteristics of worn brake pads due to silica sand embedment into their friction layers. Wear. 2016;358-359:123-136.

[7] Sinou JJ, Lenoir D, Besset S, GilIot F. Squeal analysis based on the laboratory experimental bench "Friction-Induced Vibration and noisE at Ecole Centrale de Lyon" (FIVE@ECL). Mechanical Systems and Signal Processing. 2019;119:561-588.

[8] Talotte C, Gautier PE, Thompson DJ, Hanson C. Identification, modelling and reduction potential of railway noise sources: a critical survey. Journal of Sound and Vibration. 2003;267:447-468.

[9] Sinou JJ, Loyer A, Chiello O, Mogenier G, Lorang X, Cocheteux F, et al. A global strategy based on experiments and simulations for squeal prediction on industrial railway brakes. Journal of Sound and Vibration. 2013;332:5068-5085.

[10] Brizard D, Chiello O, Sinou JJ, Lorang X. Performances of some reduced bases for the stability analysis of a disc/pads system in sliding contact. Journal of Sound and Vibration. 2011;330:703-720.

[11] Cascetta F, Caputo F, De Luca A. Squeal Frequency of a Railway Disc Brake Evaluation by FE Analyses. Advances in Acoustics and Vibration. 2018;2018:1-10.

[12] Lorang X, Foy-Margiocchi F, Nguyen QS, Gautier PE. TGV disc brake squeal. Journal of Sound and Vibration. 2006;293:735-746.

[13] Hui L, Yu D. Optimization design of a disc brake system with hybrid uncertainties. 2016;98:112-122.

[14] Wang DW, Mo JL, Liu MQ, Li JX, Ouyang H, Zhu MH, et al. Improving tribological behaviours and noise performance of railway disc brake by grooved surface texturing. Wear. 2017;376:1586-1600.

[15] Mortelette L, Brunel JF, Boidin X, Desplanques Y, Dufrénoy P, Smeets L. SAE technical paper series - impact of mineral fibres on brake squeal occurrences. Sae Brake Colloquium & Exhibition. 2009.

[16] Majcherczak D, Dufrénoy P. Dynamic analysis of a disc brake under frictional and thermomechanical internal loading. Archive of Applied Mechanics. 2006;75:497-512.

[17] Ghazaly NM, Faris WF. Optimal design of a brake pad for squeal noise reduction using response surface

methodology. International Journal of Vehicle Noise & Vibration. 2012;8:125-135.

[18] Chiello O, Sinou J-J, Vincent N, Roches GVd, Cocheteux F, Bellaj S, et al. Squeal noise generated by railway disc brakes: Experiments and stability computations on large industrial models. Journal of the Acoustical Society of America. 2013;133:3461.

[19] Tang B, Mo JL, Wu YK, Quan X, Zhu MH, Zhou ZR. Effect of the friction block shape of railway brakes on the vibration and noise under dry and wet conditions. Tribology Transactions. 2019;62:262-273.

[20] Nouby M, Srinivasan K. Simulation of the structural modifications of a disc brake system to reduce brake squeal. Proceedings of the Institution of Mechanical Engineers Part D-Journal of Automobile Engineering. 2011;225:653-672.

[21] Massi F, Baillet L, Culla A. Structural modifications for squeal noise reduction: numerical and experimental validation. International Journal of Vehicle Design. 2009;51:168-189.

[22] Chen GX, Lv JZ, Zhu Q, He Y, Xiao XB. Effect of the braking pressure variation on disc brake squeal of a railway vehicle: Test measurement and finite element analysis. Wear. 2019;426:1788-1796.

[23] Zhang L, Li W, Meng D. Influence of heterogeneous contact stiffness and heterogeneous friction coefficient on frictional squeal. Shock and Vibration. 2018;2018:1-21.

[24] Hetzler H, Willner K. On the influence of contact tribology on brake squeal. Tribology International. 2012;46(1):237-246.

[25] Lazzari A, Tonazzi D, Massi F. Squeal propensity characterization of brake lining materials through friction noise measurements. Mechanical Systems and Signal Processing. 2019;128:216-228.

[26] Cantone F, Massi F. A numerical investigation into the squeal instability: Effect of damping. Mechanical Systems and Signal Processing. 2011;25:1727-1737.

[27] Wang DW, Mo JL, Zhang Q, Zhao J, Ouyang H, Zhou ZR. The effect of the grooved elastic damping component in reducing friction-induced vibration. Tribology International. 2017;110:264-277.

[28] Lu XD, Zhao J, Mo JL, Zhang Q, Zhang X, Zhou ZR. Improvement of dynamical and tribological properties of friction systems by introducing parallel-grooved structures in elastic damping components. Composite Structures. 2018;192:8-19.

[29] Deng C, Yin J, Zhang H, Xiong X, Wang P, Sun M. The tribological properties of Cf/Cu/C composites under applied electric current. Tribology International. 2017;116:84-94.

[30] Su L, Gao F, Han X, Chen J. Effect of copper powder third body on tribological property of copper-based friction materials. Tribology International. 2015;90:420-425.

[31] Xiao Y, Zhang Z, Yao P, Fan K, Zhou H, Gong T, et al. Mechanical and tribological behaviors of copper metal matrix composites for brake pads used in high-speed trains. Tribology International. 2018;119:585-592.

[32] Noh HJ, Jang H. Friction instability induced by iron and iron oxides on friction material surface. Wear. 2018;400:93-99.

[33] Ferrer C, Pascual M, Busquets D, Rayon E. Tribological study of Fe-Cu-Cr-graphite alloy and cast iron railway brake shoes by pin-on-disc technique. Wear. 2010;268:784-789.

[34] Kchaoua M, Mat Lazimb A.R, Abdul Hamidb M.K, Abu Bakarb A.R. Experimental studies of friction-induced brake squeal: Influence of environmental sand particles in the interface brake pad-disc. Tribology International. 2017;110: 307-317.

[35] Brunetti J, Massi F, D'Ambrogio W, Berthier Y. A new instability index for unstable mode selection in squeal prediction by complex eigenvalue analysis. Journal of Sound and Vibration. 2016;377:106-122.

[36] Oberst S, Lai JCS. Pad-mode-induced instantaneous mode instability for simple models of brake systems. Mechanical Systems and Signal Processing. 2015;62-63:490-505.

[37] Soobbarayen K, Besset S, Sinou JJ. Noise and vibration for a self-excited mechanical system with friction. Applied Acoustics. 2013;74:1191-1204.

[38] Hoffmann N, Fischer M, Allgaier R, Gaul L. A minimal model for studying properties of the mode-coupling type instability in friction induced oscillations. Mechanics Research Communications. 2002;29:197-205.

[39] Pan W, Li X, Wang L, Guo N, Yang Z. Influence of contact stiffness of joint surfaces on oscillation system based on the fractal theory. Archive of Applied Mechanics. 2018;88:525-541.

[40] Pan W, Li X, Wang L, Guo N, Mu J. A normal contact stiffness fractal prediction model of dry-friction rough surface and experimental verification. European Journal of Mechanics a-Solids. 2017;66:94-102.

[41] Tonazzi D, Massi F, Salipante M, Baillet L, Berthier Y. Estimation of the normal contact stiffness for frictional interface in sticking and sliding conditions. Lubricants. 2019;7:1-17.

[42] Lyu H, Walsh SJ, Chen G, Zhang L, Qian K, Wang L. Analysis of friction-induced vibration leading to brake squeal using a three degree-of-freedom model. Tribology Letters. 2017;65:1-13.

[43] Qiao SL, Ibrahim RA. Stochastic dynamics of systems with friction-induced vibration. Journal of Sound and Vibration. 1999;223:115-140.

[44] Eriksson M, Bergman F, Jacobson S. Surface characterisation of brake pads after running under silent and squealing conditions. 1999;232:163-167.

[45] Barros LY, Neis PD, Ferreira NF, Pavlak RP, Masotti D, Matozo LT, et al. Morphological analysis of pad-disc system during braking operations. Wear. 2016;352-353:112-121.

[46] Kim JW, Joo BS, Jang H. The effect of contact area on velocity weakening of the friction coefficient and friction instability: A case study on brake friction materials. Tribology International. 2019;135:38-45.

[47] Lee S, Jang H. Effect of plateau distribution on friction instability of brake friction materials. Wear. 2018;400:1-9.

[48] Zhang P, Zhang L, Wei D, Wu P, Cao J, Shijia C, et al. Effect of graphite type on the contact plateaus and friction properties of copper-based friction material for high-speed railway train. Wear. 2019;432:38-45.

[49] Wang DW, Mo JL, Liu MQ, Onyang H, Zhou ZR. Noise performance improvements and tribological

consequences of a pad-on-disc system through groove-textured disc surface. Tribology International. 2016;102:222-236.

[50] Zhang Q, Mo JL, Lu XD, Zhao J, Wang DW, Zhou ZR. Grooved-structure design for improved component damping ability. Tribology International. 2018;123:50-60.

[51] Eriksson M, Bergman F, Jacobson S. On the nature of tribological contact in automotive brakes. Wear. 2002;252:26-36.

[52] AbuBakar A R, Ouyang H. Wear prediction of friction material and brake squeal using the finite element method. Wear. 2008; 264: 1069-1076.

[53] Yoon SW, Shin MW, Lee WG, Jang H. Effect of surface contact conditions on the stick-slip behavior of brake friction material. Wear. 2012;294:305-312.

[54] Bergman F, Eriksson M, Jacobson S. Influence of disc topography on generation of brake squeal. Wear. 1999;225:621-628.

[55] Massi F, Berthier Y, Baillet L. Contact surface topography and system dynamics of brake squeal. Wear. 2008;265:1784-1792.

[56] Lü H, Shangguan W-B, Yu D. A unified method and its application to brake instability analysis involving different types of epistemic uncertainties. Applied Mathematical Modelling. 2018; 56:158-171.

[57] Neis PD, Ferreira NF, Fekete G, Matozo LT, Masotti D. Towards a better understanding of the structures existing on the surface of brake pads. Tribology International. 2017;105:135-147.

[58] Ouyang H, AbuBakar A R, Li L. A combined analysis of heat conduction, contact pressure and transient vibration of a disk brake [J]. International Journal of Vehicle Design, 2009, 51(1/2):190-206.

[59] Oberst S, Lai JCS. Chaos in brake squeal noise. Journal of Sound and Vibration. 2011;330:955-975.

[60] Dong CL, Mo JL, Yuan CQ, et al. Vibration and Noise Behaviors During Stick–Slip Friction. Tribology Letters. 2019; 67: 1-12.

Mortelette, L. , Brunel, J. F. , Boidin, X. , Desplanques, Y. , Dufrénoy, P., & Smeets, L. Impact of Mineral Fibres on Brake Squeal Occurrences. Sae Brake Colloquium & Exhibition. 2009; 1.

Mortelette, L., Brunel, J., Boidin, X., Desplanques, Y. et al., "Impact of Mineral Fibres on Brake Squeal Occurrences," SAE Technical Paper 2009-01-3050, 2009, https://doi.org/10.4271/2009-01-3050.

List of figure captions

Fig. 21 Real part (a) and frequency (b) of the eigenvalue of the brake system

Fig. 22 Tangential (a) and normal vibration acceleration (b) of the brake system for different friction coefficients and contact inclination angles